nature chemical biology

ARTICLE

PUBLISHED ONLINE: 20 NOVEMBER 2011 | DOI: 10.1038/NCHEMBIO.715

Mechanical modulation of catalytic power on F_1-ATPase

Rikiya Watanabe[1,5], Daichi Okuno[1,5], Shouichi Sakakihara[2], Katsuya Shimabukuro[3], Ryota Iino[1], Masasuke Yoshida[4] & Hiroyuki Noji[1]*

The conformational fluctuation of enzymes has a crucial role in reaction acceleration. However, the contribution to catalysis enhancement of individual substates with conformations far from the average conformation remains unclear. We studied the catalytic power of the rotary molecular motor F_1-ATPase from thermophilic *Bacillus* PS3 as it was stalled in transient conformations far from a stable pausing angle. The rate constants of ATP binding and hydrolysis were determined as functions of the rotary angle. Both rates exponentially increase with rotation, revealing the molecular basis of positive cooperativity among three catalytic sites: elementary reaction steps are accelerated via the mechanical rotation driven by other reactions on neighboring catalytic sites. The rate enhancement induced by ATP binding upon rotation was greater than that brought about by hydrolysis, suggesting that the ATP binding step contributes more to torque generation than does the hydrolysis step. Additionally, 9% of the ATP-driven rotary step was supported by thermal diffusion, suggesting that acceleration of the ATP docking process occurs via thermally agitated conformational fluctuations.

Protein molecules experience a large number of conformational substates that vary from the average conformation as they are agitated by collisions with surrounding water molecules[1–3]. Protein conformational dynamics, especially the collective motion of residues that usually occurs on a large scale, such as in domain rotation, is considered to be important for enhancement of the catalytic power of enzymes. Conformational dynamics are believed to have a critical role in the preferential binding of the transient state, which is the general mechanism of catalysis enhancement by enzymes[4]. The classic models for substrate docking are the induced-fit model and the conformational selection model[5–7]. These models are also based on the conformational plasticity and dynamics of the protein. Although there is a great deal of experimental evidence supporting the contribution of conformational dynamics to the enhancement of reactions[3,7], the catalytic power of individual conformational substates is not well understood. In the present study, we investigated the catalytic power of F_1-ATPase as it was stalled in transient conformations deviating far from conformations at equilibrium.

F_1-ATPase (F_1) is a rotary motor protein that hydrolyzes ATP to rotate the rotor γ subunit against the surrounding stator of the $\alpha_3\beta_3$ ring[8–12]. The catalytic sites of F_1 are located at three α-β interfaces, mainly on β subunits[13]. F_1 performs 120° counterclockwise (viewed from the membrane side), stepwise rotations, and each step occurs upon a net single turnover of ATP hydrolysis[14]. The 120° step is further divided into 80° and 40° substeps[15]. The 80° substep is triggered upon ATP binding and ADP release, whereas the 40° substep occurs after ATP hydrolysis and the release of inorganic phosphate (P_i)[15–17]. We use the terms binding angle and catalytic angle to indicate the rotary angles at which the 80° and 40° substeps start, respectively. The elementary reactions driving each substep occur on different β subunits. The present reaction scheme of catalysis and rotation is shown in **Figure 1a**. If a β subunit's ATP binding angle is defined as 0°, it executes a hydrolysis reaction after γ rotation between 0° and 200° and releases ADP and P_i at 240° and 320°, respectively[18].

The principal physiological role of this protein involves the reverse reaction—that is, ATP synthesis. In a cell, F_1 forms ATP synthase by binding to the F_o motor, which is the membrane-embedded portion of ATP synthase and a rotary motor driven by proton flux down the proton motive force. The F_o motor rotates the γ subunit of F_1 in reverse, forcing F_1 to catalyze ATP synthesis from ADP and P_i. ATP synthesis via the mechanical reverse rotation of F_1 has been experimentally confirmed[19,20]. These observations imply that ATP synthesis can occur against the large free energy of ATP hydrolysis, which is around −54 kJ mol^{-1}, only by manipulating the angular position of the γ subunit. The reversibility of mechanochemical coupling is a remarkable feature of F_1 that distinguishes it from other molecular motors[21–23].

To achieve the high reversibility of mechanochemical coupling, the kinetics and chemical equilibrium of the individual reaction steps comprising ATP hydrolysis on F_1 inevitably have to be modulated in response to the γ rotation[16,24,25]. As mentioned above, F_1 has two stable conformational states: the binding dwelling state and the catalytic dwelling state. Although the basic kinetic properties of these two stable states have been well characterized[15,16,18,26,27], the extent to which the kinetic power of F_1 is modulated upon γ rotation remains elusive. Thus, elucidation of the kinetic properties of transient conformational states during γ rotation is essential to understanding the mechanochemical coupling mechanism of F_1. In a previous study, direct measurement of the kinetics of F_1 in transient conformational states was conducted for the ADP-release step of a catalytically inactive F_1, the so-called ADP-inhibited form[28]. When F_1 strongly binds ADP, it lapses into ADP inhibition, which pauses the rotation[29]. When forcibly stalled in the forward angle with magnetic tweezers, F_1 releases a bound ADP and resumes active rotation. Kinetic analysis of this phenomenon revealed that the dissociation rate, or off rate, of ADP increases exponentially upon γ rotation, demonstrating the critical role that the transient conformational state plays in the acceleration of the reaction.

[1]Department of Applied Chemistry, School of Engineering, University of Tokyo, Tokyo, Japan. [2]Institute of Scientific and Industrial Research, Osaka University, Osaka, Japan. [3]Department of Biological Science, Florida State University, Tallahassee, Florida, USA. [4]Department of Molecular Biosciences, Faculty of Life Sciences, Kyoto Sangyo University, Kyoto, Japan. [5]These authors contributed equally to this work *e-mail: hnoji@appchem.t.u-tokyo.ac.jp

In the present study, we performed the stalling experiment to elucidate how catalytically active F_1 modulates the rate and equilibrium constants of ATP binding and hydrolysis. The results revealed that both reactions, particularly the ATP binding step, are distinctly accelerated upon forward rotation, whereas the reactions were suppressed in the backward direction. These findings present important implications for the molecular mechanisms of torque generation and catalytic cooperativity among three catalytic β subunits. The role of thermal conformational fluctuation in catalytic acceleration was also determined.

RESULTS

Manipulation of single F_1 rotation

A magnetic bead (ϕ ~200 nm) was attached to the γ subunit of F_1 molecules immobilized on a glass surface to observe and manipulate the rotary motion of the γ subunit under a bright field (**Fig. 1b**). Single-molecule manipulation was conducted using a pair of magnetic tweezers[20,28]. Owing to the viscous load imposed on the magnetic bead, the maximum rotational velocity was around 5 Hz[25]. Accordingly, the catalytic dwell of 1- to 2-ms duration[15,16] could not be detected in the rotation assay. For the stalling experiments, F_1 rotation was observed under conditions in which the rotational pause caused by ATP binding dwell or hydrolysis dwell was lengthened enough to enable recording at a video rate of 30 frames per second by decreasing ATP concentration or by using a mutant F_1, an ATP analog or both (described further below). When F_1 was paused, the tweezers were turned on to stall the magnetic bead at the target angle (**Fig. 1c**). After the set period had elapsed, the tweezers were turned off to release F_1. If the reaction occurred during stalling and F_1 subsequently generated the torque to move the rotor to the next pause angle, F_1 would move to the next pause angle immediately after being released from the magnetic tweezers. If the reaction had not yet taken place, F_1 would return to the original pause angle until the reaction occurred. The former and latter behaviors are referred to as 'on' and 'off', respectively. **Figure 1d** shows examples of the time course in the ATP binding measurement (also shown in **Supplementary Movies 1** and **2**). In rare cases, irregular behaviors such as pausing at the angle of release were observed. These phenomena were seen when F_1 was stalled at angles over ±50° from the binding angle in the ATP binding experiment or at angles over ±70° from the catalytic angle in the hydrolysis experiment. Therefore, measurements were primarily conducted in the angle range of either ±50° for ATP binding measurements or ±70° for the hydrolysis measurements to avoid such behaviors. The following sections discuss the analysis of the probability of an on event against total trials, P_{ON}.

Angle dependence of ATP binding

Experiments were conducted at 20 nM, 60 nM and 200 nM ATP with ATP waiting times of 2.6 s, 0.92 s and 0.33 s, respectively. **Figure 2a** shows P_{ON} at 60 nM ATP plotted against the stall angle. P_{ON} increased with both the stall angle and stall time. This finding is similar to our previous observation of ADP release from an ADP-inhibited F_1 molecule[28]. P_{ON} for each stall angle was replotted against the stall time to provide the time courses of ATP binding (**Fig. 2b** and **Supplementary Results**, **Supplementary Fig. 1**). Although P_{ON} increased with stall time (unlike the aforementioned ADP release), P_{ON} did not always indicate 100% saturation but showed convergence to a certain value, for example, 70% for a −10° stall (**Fig. 2b**). These observations imply that ATP binding is reversible and that ATP release also occurs during stalling. Accordingly, the plateau level indicates the equilibrium between ATP binding and release. To confirm the reversibility, we analyzed the dwell time of F_1 to spontaneously conduct a 120° step after an off event. Here only experiments with longer stalling times in which P_{ON} achieved a plateau were analyzed to avoid including data collected before equilibrium was reached. The obtained dwell-time histograms showed a single exponential decay, providing the rate constant (**Supplementary Fig. 2**). As expected, the determined rate constants were dependent on ATP concentration and corresponded to the rate constants for free rotation (**Fig. 2c** and **Supplementary Fig. 2**). This correspondence excludes the possibility that unexpected inactivation occurred during stalling to compete with the ATP binding process. Had inactivation occurred, the spontaneous 120° step rotation after the off event would have been initiated by at least two reaction steps: spontaneous reactivation from the inactive state and ATP binding, which would result in the dwell time's deviation from a simple exponential distribution or dependence on ATP concentration. We also plotted a histogram of the dwell time of F_1 to conduct the second 120° step after the on event (**Fig. 2c** and **Supplementary Fig. 2**). The good agreement of these histograms

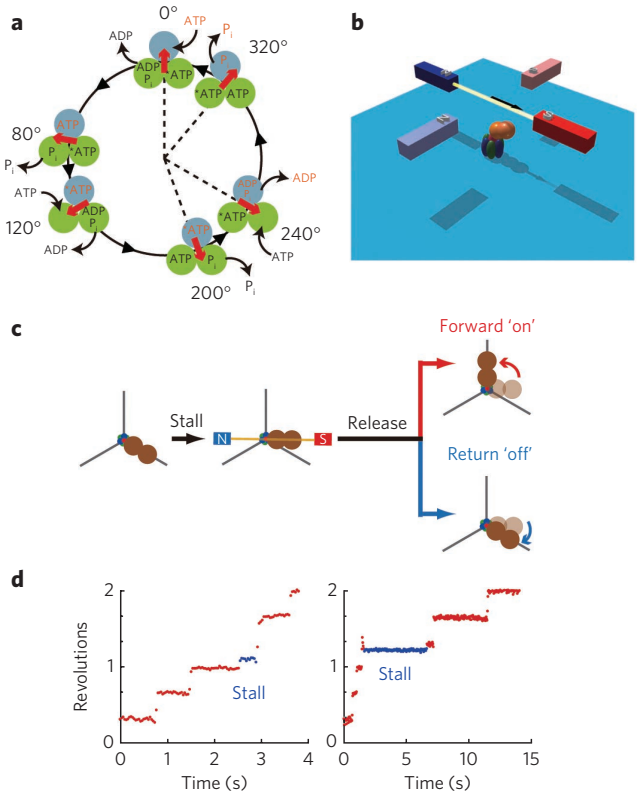

Figure 1 | Experimental setup and procedure for manipulation of the F_1 motor. (**a**) Chemomechanical coupling scheme of F_1. The circles and red arrows represent the catalytic states of β subunits and the angular positions of γ subunits. Each β subunit completes a single turnover of ATP hydrolysis with one turn of γ, whereas in the catalytic phase, three β subunits differ by 120°. The catalytic state of the top β subunit (cyan) is provided for clarification. ATP binding, hydrolysis, ADP release and P_i release occur at 0°, 200°, 240° and 320°, respectively. (**b**) Schematic image of the experimental setup (not to scale). (**c**) Experimental procedures for stalling experiment. When F_1 paused the ATP binding dwell or hydrolysis dwell, the tweezers were turned on to stall F_1 at the target angle and then were turned off to release the motor after the set period lapsed. A released motor shows rapid forward stepping (on) or a return to the original pause angle (off), behaviors indicating that the reaction under investigation is either complete or incomplete, respectively. (**d**) Examples of stalling experiment for ATP binding at 60 nM ATP. During a pause, F_1 was stalled at +30° from the binding angle for 0.5 s and then released (**Supplementary Movie 1**, left side). After being released, F_1 stepped to the next binding angle without moving back, indicating that ATP had already bound to F_1. When stalled at −30° for 5 s (**Supplementary Movie 2**, right side), F_1 rotated back to the original binding angle, indicating that no ATP binding had occurred.

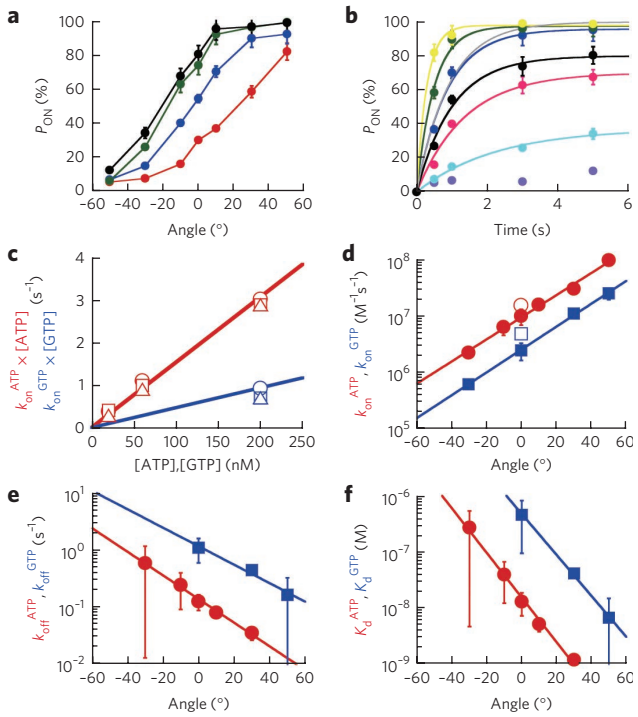

Figure 2 | Angle dependence of ATP binding. (**a**) Angle dependence of P_{ON} at 60 nM ATP. The 0° represents the original binding angle before manipulation. The stall times were 0.5 s (red), 1 s (blue), 3 s (green) and 5 s (black). Each data point was obtained from 39–536 trials using 13–32 molecules. (**b**) Time courses of P_{ON}. The data in **Figure 2a** were replotted against stall time: −50° (purple), −30° (cyan), −10° (pink), 0° (black), +10° (blue), +30° (green) and +50° (yellow). Gray line represents the time course in free rotation. The k_{on}^{ATP} and k_{off}^{ATP} were determined by fitting with a single exponential function, $\{k_{on}^{ATP}[ATP] / (k_{on}^{ATP}[ATP] + k_{off}^{ATP})\}[1 - \exp\{-(k_{on}^{ATP}[ATP] + k_{off}^{ATP})t\}]$, according to the reversible reaction scheme $F_1 + ATP \rightleftarrows F_1 - ATP$. (**c**) Rate constants determined from the histograms of ATP (red) or GTP (blue) binding dwell in free rotation (circles) for F_1 after either an off (triangles) or an on (squares) event. Histograms are given in **Supplementary Figures 2** and **4**. The red and blue lines represent the rate constants k_{on}^{ATP} (1.5×10^7 M^{-1} s^{-1}) and k_{on}^{GTP} (4.6×10^6 M^{-1} s^{-1}), respectively. (**d**–**f**) Angle dependence of k_{on} in **d**, k_{off} in **e** and K_d in f. Red and blue symbols represent the values for ATP and GTP determined from **Figure 2b** and **Supplementary Figures 1** and **4**. Angle dependences determined by fitting are shown in **Table 1**. In **d**, open symbols represent k_{on} in free rotation. Error bars, s.d.

with those measuring free rotation confirmed that manipulation did not alter the kinetic properties of F_1. However, when stalled for a period much longer than the time in which ATP binding and release reach to the equilibrium state, F_1 occasionally lapsed into a peculiar pausing state, fluctuating between 0° and −40°, similar to the inactive state found at subnanomolar ATP concentrations[30]. The probability of occurrence of this inactive state was higher at lower concentrations of ATP and after longer stalling times. The probability of the inactive state was, however, negligible (that is, less than 5%) during the 16-s stalling at +10° at 20 nM ATP. Therefore, we omitted this event from the data analysis.

By fitting time courses of P_{ON} on the basis of a reversible reaction scheme, the rate constants of ATP binding and release, k_{on}^{ATP} and k_{off}^{ATP}, were determined for each stall angle (**Fig. 2d**,**e** and **Supplementary Fig. 3**). As expected, the rate constants at each stall angle did not vary, regardless of the ATP concentration. Whereas k_{on}^{ATP} increased exponentially with stall angle by about 15-fold from −30° to +30°, k_{off}^{ATP} decreased exponentially by a factor of 18. The dissociation constant of ATP, K_d^{ATP}, decreased by a factor of 235 from −30° to +30° (**Fig. 2f**). Angle dependences are summarized in **Table 1**.

Table 1 | Angle dependence of kinetic parameters

	Angle dependence
k_{on}^{ATP} (M^{-1} s^{-1})	$(9.2 \pm 0.6) \times 10^6 \times \exp[(0.045 \pm 0.002) \times \theta]$
k_{off}^{ATP} (s^{-1})	$(0.14 \pm 0.008) \times \exp[(-0.048 \pm 0.002) \times \theta]$
k_a^{ATP} (M^{-1})	$(6.5 \pm 0.5) \times 10^7 \times \exp[(0.091 \pm 0.002) \times \theta]$
k_d^{ATP} (M)	$(1.5 \pm 0.08) \times 10^{-8} \times \exp[(-0.091 \pm 0.002) \times \theta]$
k_{on}^{GTP} (M^{-1} s^{-1})	$(2.5 \pm 0.06) \times 10^6 \times \exp[(0.047 \pm 0.0008) \times \theta]$
k_d^{GTP} (s^{-1})	$(1.2 \pm 0.06) \times \exp[(-0.037 \pm 0.004) \times \theta]$
k_{off}^{GTP} (M)	$(4.7 \pm 0.02) \times 10^{-7} \times \exp[(-0.084 \pm 0.0012) \times \theta]$
k_{hyd}^{ATP} (s^{-1})[a]	$(3.6 \pm 0.3) \times \exp[(0.019 \pm 0.002) \times \theta]$
k_{syn}^{ATP} (s^{-1})[a]	2.1 ± 0.13
$K_E^{Hyd-ATP}$ [#]	$(1.8 \pm 0.07) \times \exp[(0.018 \pm 0.0008) \times \theta]$
$k_{hyd}^{ATP\gamma S}$ (s^{-1})[a]	$(0.17 \pm 0.03) \times \exp[(0.020 \pm 0.001) \times \theta]$
$k_{syn}^{ATP\gamma S}$ (s^{-1})[a]	0.19 ± 0.02
$K_E^{Hyd-ATP\gamma S}$ [a]	$(0.85 \pm 0.06) \times \exp[(0.016 \pm 0.002) \times \theta]$

[a]Determined using a mutant, $F_1(\beta^{E190D})$.

Angle dependence of GTP binding

To assess the generality of the above findings, we measured the affinity of F_1 for GTP, whose on rate is 3.3 times slower than that of ATP[31]. P_{ON} of GTP binding also showed reversible binding and release (**Supplementary Fig. 4**), giving both k_{on}^{GTP} and k_{off}^{GTP}. Notably, although the absolute values of both k_{on}^{GTP} and k_{off}^{GTP} were different from those of ATP, GTP binding and release showed essentially the same angle dependences, as indicated by their almost identical slopes in the plot (**Fig. 2d**,**e**). K_d^{GTP} also showed the same angle dependence (**Fig. 2f**). Thus, mechanical modulation of ligand binding was revealed to be intrinsically programmed in F_1.

Angle dependence of hydrolysis

For wild-type F_1, the dwell time for hydrolysis is only 1 ms[15,16], which is too short for the stalling experiment. Therefore, we conducted the stalling experiment using the hydrolysis reaction of the ATP analog ATPγS and a mutant F_1, $F_1(\beta^{E190D})$, both of which retard the hydrolysis step. Their combination reduces the hydrolysis reaction rate by a factor of 10,000 (ref. 17). In the presence of ATPγS, $F_1(\beta^{E190D})$ showed a 120° stepping rotation with a hydrolysis pause of 9.1 s. Magnetic tweezers were used to stall F_1 in the hydrolysis pause to determine P_{ON}. As shown in the previous study[18], P_{ON} increased in two phases. After the rapid increase, P_{ON} gradually approached 100% (**Fig. 3a**). The first increase was almost complete within 10 s, consistent with the time constant of ATPγS hydrolysis. The second increase was extremely slow for an effective catalytic reaction. We previously showed that this slow increase was a result of the release of thiophosphate ($thioP_i$), which is produced during ATPγS hydrolysis on the β subunit at the 200° state during stalling[18]. This slow release of $thioP_i$ is an uncoupled side reaction that is suppressed by the presence of 10 mM $thioP_i$ (**Supplementary Fig. 5**). During normal catalysis (that is, in the absence of external force), P_i is released from the β subunit in the 320° state[18]. We fitted the time courses of P_{ON} using a consecutive reaction model in which the reversible hydrolysis step is followed by irreversible $thioP_i$ release from the β subunit at the 200° state: F_1-ATPγS → F_1-ADP-$thioP_i$ → F_1-ADP + $thioP_i$ (**Supplementary Methods**). The rate constants of hydrolysis and synthesis, $k_{hyd}^{ATP\gamma S}$ and $k_{syn}^{ATP\gamma S}$, and the rate constant of thioPi release, k_{off}^{thioPi}, were determined from the fitted data. Notably, whereas $k_{hyd}^{ATP\gamma S}$ increased with the rotary angle, $k_{syn}^{ATP\gamma S}$ remained constant around 0.19 s^{-1} (**Fig. 3b**). The equilibrium constant of hydrolysis ($k_{hyd}^{ATP\gamma S} / k_{syn}^{ATP\gamma S} = K_E^{Hyd-ATP\gamma S}$) has relatively weak angle dependence compared with the equilibrium constant of

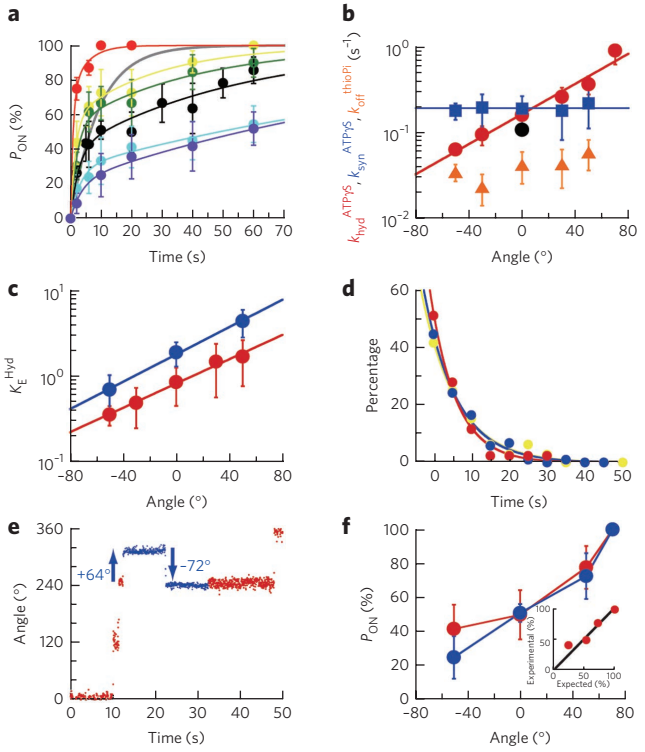

Figure 3 | Angle dependence of the hydrolysis step. (**a**) Time course of P_{ON} of $F_1(\beta^{E190D})$ at 1 mM ATPγS after stalling at −50° (purple), −30° (cyan), 0° (black), +30° (green), +50° (yellow) and +70° (red) from the original catalytic angle; data were fitted as described in **Supplementary Methods**. Gray line represents the time course in free rotation. Each data point was obtained from 12–102 trials using 4–15 molecules. (**b**) Angle dependence of $k_{hyd}^{ATP\gamma S}$ (red), $k_{syn}^{ATP\gamma S}$ (blue) and k_{off}^{thioPi} (orange). Angle dependences determined by fitting are shown in **Table 1**. The black circle indicates $k_{hyd}^{ATP\gamma S}$ in free rotation. (**c**) Angle dependence of the equilibrium constant of hydrolysis, K_E^{Hyd}, for ATPγS (red) and ATP (blue). (**d**) Histograms of the catalytic dwell in free rotation (yellow) for F_1 after either an off (blue) or an on (red) event. The rate constants were determined to be 0.11 s^{-1} (yellow), 0.15 s^{-1} (blue) and 0.12 s^{-1} (red) by fitting with exponential decay. (**e**) Time course of an experiment to confirm the reversibility of the hydrolysis step. F_1 in a catalytic dwell stalled around +70° for 10 s and then rotated back to the indicated angle to be stalled again for 10 s. Blue points show the period under manipulation. (**f**) Probability of resynthesis of ATPγS determined experimentally from data in **Figure 3e** (red) and calculated mathematically from data in **Figure 3a** (blue). The inset shows a correlation between experimental and expected values determining the efficiency of reversibility (~95%). Error bars, s.d.

ATP binding (**Fig. 3c**). The k_{off}^{thioPi} value at ~200° was found to be constant around 0.04 s^{-1}, in agreement with the contention that P_i release at 200° is not coupled with γ rotation[18].

To confirm the reversibility of ATPγS hydrolysis, we analyzed the dwell time of the spontaneous 120° step from the original catalytic angle after an off event. We also evaluated the catalytic dwell time of the 120° step from the next catalytic angle after an on event. In both cases, the dwell-time histograms were in good agreement with those for free rotation (**Fig. 3d**). The reversibility of the hydrolysis step was further verified. F_1 was stalled at +70° for 10 s to fully induce ATPγS hydrolysis. Next, F_1 was forcibly rotated back to the targeted angle, from −50° to +70°, to stall for 10 s to reverse the reaction (**Fig. 3e**). The resultant probability that the released F_1 showed the catalytic pause at the original catalytic angle coincided with the expected values (**Fig. 3a**,**f**).

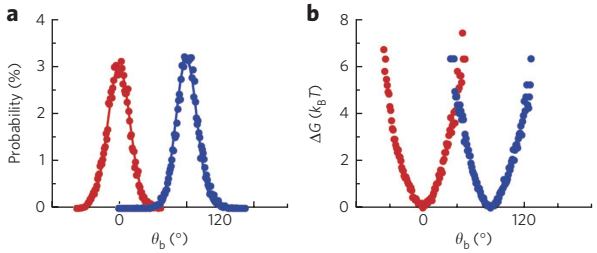

Figure 4 | Probability density of rotary angle and rotary potential of pausing F_1. (**a**) The probability densities of the rotary angle in the binding dwell of wild-type F_1 at 200 nM ATP (red) and the catalytic dwell of $F_1(\beta^{E190D})$ at 1 mM ATP or 1 mM ATPγS (blue). The data were obtained from 6–7 observations for each condition and fitted with Gaussian curves; $P(\theta) = 3.0 \times \exp(-\theta^2 / 345)$ for ATP binding dwell and $P(\theta) = 3.0 \times \exp(-(\theta - 80)^2 / 323)$ for hydrolysis dwell. The binding and catalytic angles were assigned as 0° and 80°, respectively. (**b**) Rotary potentials of F_1 in the binding dwell (red) and the catalytic dwell (blue). The rotary potentials were calculated from the probability densities shown in **Figure 4a** according to Boltzmann's law.

To confirm the weak angle dependence of the hydrolysis step under different conditions, the stalling experiment was also conducted for the ATP hydrolysis reaction using $F_1(\beta^{E190D})$ (**Supplementary Fig. 6**), and the resulting time constant of the hydrolysis step was 0.32 s. A two-phase increase in the time course of P_{ON} was again observed. The rate constants k_{hyd}^{ATP} and k_{syn}^{ATP} and the equilibrium constant $K_E^{Hyd\text{-}ATP}$ were determined in the same fashion as those measured for ATPγS hydrolysis. The determined equilibrium constant of ATP hydrolysis showed essentially the same angle dependence as that of ATPγS hydrolysis using $F_1(\beta^{E190D})$ (**Fig. 3c**). Thus, the weak angle dependence of the hydrolysis is inherent in F_1.

Thermal reaction acceleration

On the basis of the angle dependences determined for the ATP binding and hydrolysis steps, we attempted to estimate the role of the catalytic power of the transient conformational state in the reaction acceleration in the absence of external force. The probability density of the rotary angle was measured from rotational Brownian motion during the ATP waiting state or the hydrolysis waiting state (**Fig. 4a**). The rotary potentials were determined from the probability density according to Boltzmann's law (**Fig. 4b**). Both potentials were similar to each other and were essentially the same as previously reported[32]. Next, the mean rate constant of ATP binding or hydrolysis during the dwell in free rotation was computed from the probability density, $P(\theta)$, and the angle-dependent rate constant, $k(\theta)$, using the following equation: $\langle k \rangle = \int k(\theta)\, P(\theta)\, d\theta$. In this computation, the reverse reaction was not considered because the traveling time constant of the 120° step, 50 ms, is much shorter than the time constant for the reverse reactions. The calculated rate constants are shown in **Table 2**. These values were in good agreement with the actual rate constants determined from free rotation, supporting the validity of the stalling experiments. Interestingly, the rate constant of ATP binding without the external force (**Fig. 2d**) was higher than that observed when the γ was stalled at the center of the pause angle (±0°). This phenomenon is similar to the release of ADP from ADP-inhibited F_1 (ref. 28) and is attributed to thermal agitation. When free from external forces, F_1 undergoes rotational Brownian motion around the pause angle when it is paused. When γ is thermally pushed forward, the probability of ATP binding increases exponentially, and F_1 binds to an ATP molecule from the solution. Conversely, thermal fluctuation did not lead to the acceleration in hydrolysis rate, owing to the smaller angular dependence of the hydrolysis rate (**Fig. 3b**). The average angles at which ATP binding and hydrolysis

Table 2 | Computation of ATP binding, hydrolysis rates and average angles from $P(\theta)$ and $k(\theta)$

		Experimental rate constant	Calculated rate constant	Average angle
ATP binding		1.5×10^7 (M^{-1} s^{-1})	1.1×10^7 (M^{-1} s^{-1})	+7.2°
Hydrolysis[a]	ATP	3.1 (s^{-1})	3.9 (s^{-1})	+3.2°
	ATPγS	0.11 (s^{-1})	0.17 (s^{-1})	+3.1°

[a]Determined using a mutant, $F_1(\beta^{E190D})$.

occur under thermal agitation were also calculated using the equation $\int\theta k(\theta)P(\theta)d\theta$ / $\int k(\theta)P(\theta)d\theta$. The average angles for ATP binding and hydrolysis were +7.2° and +3.2° from each pause angle, respectively (**Table 2**). Thus, thermal agitation accelerates the reaction, especially during the ATP binding process.

DISCUSSION

All kinetic parameters determined in this study, as well as the on and off rates of P_i determined in previous studies, are shown in **Figure 5a–c**[16,18]. Data points are plotted in the angular diagram of the reaction scheme for one β subunit, where the pause angles for ATP binding, hydrolysis, ADP release and P_i release were assigned as 0°, 200°, 240° and 320°, respectively[18]. Because it is highly probable that the actual γ position is deviated from the bead position because the system has elastic elements (for example, the outwardly protruding domain of γ, streptavidin and the $\alpha_3\beta_3$ stator ring[32,33]), we corrected angle dependences on the basis of the stiffness of the outer or inner parts of the system (**Fig. 5a–c** and **Supplementary Methods**). Regardless of this correction, all of the kinetic parameters of reactions in the hydrolysis direction show exponential acceleration upon γ rotation. This observation provides a good explanation for the cooperative ATP hydrolysis reaction mechanism among the three β subunits. When the γ subunit approaches the binding angle, ATP binding and ADP release are triggered on the β subunits in the 0° and 240° states, respectively. When these reactions are completed, the 80° substep is then triggered. Next, this 80° substep stimulates the β subunit in the 200° or 320° state to induce hydrolysis or P_i release, and the 40° substep rotation starts, which in turn initiates the second round of catalysis. Thus, each catalytic step pushes other reactions via the γ rotation.

The mechanical interplay among catalytic sites is also found in linear motor proteins. Myosin V and conventional kinesin carry two catalytic head domains that are connected by a linker domain, and the tension exerted on the linker has a key role in cooperative catalysis, suppressing catalysis on the front head or promoting that on the rear head[34]. In a more general sense, mechanical interplay among multicatalytic sites is the basic principle of allosterism. Thus, the observed mechanical modulation of catalytic properties by F_1 represents common features of enzyme allosterism.

Rotary fluctuation analysis reveals that ATP binding is induced by a thermally agitated rotation of +7.2°, which is followed by the downhill rotation on the potential slope of the ATP-bound state. This implies that ATP binding proceeds in a manner that integrates the induced fit and the pre-existing conformational selection models[35,36]. Conversely, hydrolysis does not depend on thermal agitation as much as ATP binding does because of the relatively weak angle dependence of the hydrolysis process. Even if the angle dependences are corrected with respect to the γ elasticity, these values do not change because the corrected stiffness compensates for the angle dependence of the reactions.

The observed angle dependences of the reactions suggest that F_1 operates the catalytic reactions in a more stochastic fashion than previously thought for conventional reaction schemes in which each catalytic reaction is assigned at a specific rotary angle. This implies that the individual reaction steps take place over a wide range of rotary angles. A suggestive phenomenon was found in a previous study in which F_1 was reported to hydrolyze ATP at −80° from the catalytic angle[37]. This stochastic coupling provides new insight into how F_oF_1-ATP synthase manages the structural asymmetric mismatch between F_1 and F_o. Specifically, the former has a three-fold rotary potential minima, whereas the latter has non–three-fold symmetry in most cases[38]. Even if F_1 pauses at angles that are different from its intrinsic stable angles to balance the two rotary potentials, it is still able to exert catalytic reactions. Thus, the wide range of rotary angles for triggering catalysis is one explanation for the smooth coupling between F_1 and F_o.

The present data imply that the reaction scheme for ATP synthesis is not a simple reversal of the ATP hydrolysis scheme. The probability that a bound nucleotide remains as ATP at 200° is only 37%. This value is too low to explain the efficient ATP synthesis of F_1 (ref. 20).

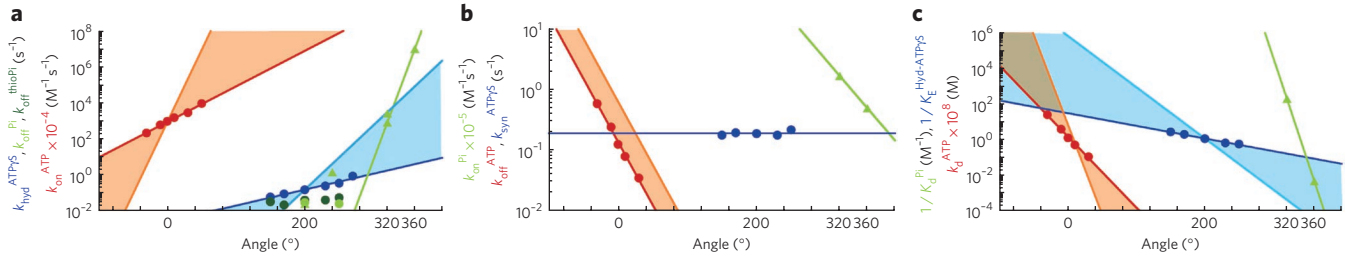

Figure 5 | Modulation of kinetic parameters upon γ rotation. (**a**) Modulation of hydrolysis reactions upon rotation. All data points are plotted along the reaction scheme for one β subunit, and the angles for ATP binding, hydrolysis and P_i (or thioP_i) release are assigned as 0°, 200° and 320°, respectively. Red circles represent k_{on}^{ATP}, blue circles represent $k_{hyd}^{ATP\gamma S}$, and light and dark green circles represent k_{off}^{Pi} and k_{off}^{thioPi}, respectively. Light green triangles represent k_{off}^{Pi} at 200°, 240°, 320° and 360° as determined in previous studies[16,18]. Solid lines represent the linear regression for k_{on}^{ATP} (red), $k_{hyd}^{ATP\gamma S}$ (blue) and k_{off}^{Pi} (light green). k_{off}^{Pi} was only fitted at 320° and 360°. Light orange or light blue lines represent the corrected regressions for k_{on}^{ATP} and $k_{hyd}^{ATP\gamma S}$ based on the elasticity of the γ subunit (**Supplementary Methods**). (**b**) Modulation of elementary steps for synthesis reactions upon rotation. Red, blue and light green represent k_{off}^{ATP}, $k_{syn}^{ATP\gamma S}$ and k_{on}^{Pi}, respectively. The light orange line represents the corrected regressions for k_{off}^{ATP} based on the elasticity of the γ subunit (**Supplementary Methods**). (**c**) Modulation of equilibrium constants upon rotation. Red, blue and light green symbols represent the dissociation constant of ATP (K_d^{ATP}), the inverse values of the equilibrium constant of ATPγS hydrolysis ($1 / K_E^{Hyd\text{-}ATP\gamma S}$), and the inverse values of dissociation constant of P_i ($1 / K_d^{Pi}$), respectively.

The value of K_d^{ATP} at 0°, $K_d^{ATP}(0°)$, is ~15–69 nM, which is also too low for efficient ATP synthesis to occur. Under physiological conditions, F_1 should release ATP in the presence of millimolar concentrations of ATP. The explanation for these points is that actual ATP synthesis or release occurs when γ is rotated far away from the catalytic or binding angle in the clockwise direction. These findings are consistent with those of a biochemical study showing that the proton-motive force enhances the release of ATP into solution[39]. Thus, the angular positions of the elementary steps for synthesis reactions should be shifted clockwise as compared with those for hydrolysis reactions. It is also likely that in the entire F_oF_1 complex, interactions with other subunits such as the ε subunit enhance and modulate the reaction equilibrium to facilitate ATP synthesis[20,40].

The observed angle dependences also present implications about the relative contribution of ATP binding and hydrolysis to torque generation. Torque generated in the ATP binding process is determined by the slope of the rotary potential of F_1 in the ATP-bound state[41]. Because $-k_BT \ln k_{off}^{ATP}$ represents the relative energy difference between the ATP-bound state and the transition state of ATP binding and release, the measure of its differential form against angle $-k_BT\ \delta/\delta\theta\ [\ln k_{off}^{ATP}(\theta)]$ is a barometer of the magnitude of torque generated upon ATP binding, although for precise estimation, the angle dependence of the energy of the transition state has to be taken into account. The exponential decay of k_{off}^{ATP} observed upon rotation indicates the constant stabilization of the F_1–ATP complex with rotation (that is, constant torque generation with rotation). This feature is consistent with the constant torque irrespective of angle and is advantageous for the efficient conversion of binding energy into mechanical work to avoid energy dissipation. That k_{off}^{ATP} has a larger angle dependence than k_{syn}^{ATP} and $k_{syn}^{ATPγS}$ means that the ATP binding process contributes to torque generation much more than hydrolysis. The angle dependence of the off rate for GTP supports this contention; k_{off}^{GTP} showed essentially the same angle dependence as ATP even though GTP is a low-affinity substrate for F_1. Accordingly, the torque of GTP-driven rotation is the same as that of ATP-driven rotation[31]. Measuring the angle dependence of the catalytic power is a unique approach to elucidate the mechanochemical coupling mechanism and opens up a new experimental direction not only for F_1 but also for other molecular motors.

The simultaneous imaging of the γ rotation and fluorescent nucleotide binding and dissociation established that two of three catalytic sites on F_1 are always occupied by nucleotides and that ATP binding to the third site induces ADP release and γ rotation[16,42]. Thus, the $K_d^{ATP}(0°)$ of ~15–69 nM determined in this study represents the affinity of the third site for ATP. On the other hand, biochemical experiments repeatedly show that the K_d^{ATP} of the third site (K_{d3}) is around 40 μM (ref. 43). This value evidently contradicts not only $K_d^{ATP}(0°)$ but also the aforementioned observation that F_1 stably holds the bound ATP at the third site for several seconds under conditions of ~10–50 nM ATP[16]. The most likely explanation for this apparent discrepancy is that the rotary angle of γ for K_{d3} is different from the ATP binding angle. According to recent intensive work on the nucleotide titration of the third site in parallel with ATPase measurement[44], ATPase rate (= rotational velocity) saturates at ATP concentrations less than K_{d3} (that is, the K_M value for ATPase activity, 6.8 μM, is evidently lower than K_{d3}). Because F_1 predominantly pauses at the catalytic angle (−40° from the ATP binding angle) when the concentration of ATP is higher than K_M[15], it is likely that K_{d3} represents the affinity of the catalytic state at −40°, which corresponds to $K_d^{ATP}(-40°)$ in this study[16,18]. Considering the strong angle dependence of K_d^{ATP}, it is reasonable that $K_d^{ATP}(0°)$ is smaller than K_{d3}. The $K_d^{ATP}(-40°)$ estimated from the angle dependence is ~590 nM–720 μM. Although the estimation has a large range, it covers the reported K_{d3} well. Thus, the apparent discrepancy can be attributed to the different angular positions for $K_d^{ATP}(0°)$ and K_{d3}. To confirm this point, direct verification of ATP binding at the 320° state is required.

Another issue that remains to be clarified is the reason for the high reversibility of the reactions. ADP release can occur simultaneously with ATP binding because it is believed to occur on the β subunit of the 240° state[16]. Although the exact rotary angle for ADP release remains to be confirmed[45], the reversibility is not easily explained. Once F_1 releases ADP during stalling, it is not able to return to the ADP-bound state because the solution contains only contaminating ADP derived from ATP (<5% of ATP). One possible explanation for this is that the actual rotary angle for ADP release is far from the binding angle and is much larger than 240°. Another potential explanation is that F_1 can return to the kinetically identical ATP-waiting state even if ADP is absent from another catalytic site. This would mean that F_1 exerts torque only when both ATP binding and ADP release have been completed. The hydrolysis step also showed high reversibility, as in our previous study[18], and a similar explanation is possible for this apparent reversibility: F_1 would exert torque, but only after both hydrolysis and P_i release occur. This explanation assumes that the $\alpha_3\beta_3$ stator ring has intrinsic cooperativity that allows three β subunits to simultaneously generate torque. By using high-speed atomic-force microscopy, we recently revealed that the isolated $\alpha_3\beta_3$ stator ring shows a highly cooperative power stroke among three β subunits[46]. The structural basis of the intrinsic cooperative power stroke is the remaining focal issue requiring elucidation.

METHODS

Rotation assay. Wild-type F_1 and $F_1(\beta^{E190D})$ derived from thermophilic *Bacillus* PS3 were prepared and assayed in the rotation experiments as previously described[18]. For rotation assay at 200 nM ATP or below, we mixed an ATP-regenerating system of 0.1 mg ml^{-1} pyruvate kinase and 1 mM phosphoenolpyruvate into the assay solution. The rotation of the magnetic beads attached to the γ subunit of F_1 was then observed under a bright-field microscope (IX-70; Olympus) with a 100× objective. Although the mean diameter of the magnetic bead was 0.73 μm according to the manufacturer (Seradyn), the actual diameter showed large variations. Small rotating beads (ϕ ~ 200 nm) were selected and analyzed because they tend to rotate smoothly, owing to the low possibility of contact with glass surfaces.

Manipulation with magnetic tweezers. Magnetic tweezers (composed of two pairs of electromagnets) were built onto the microscope stage and controlled with a custom-made program (Library). When F_1 paused at a binding angle (for ATP binding measurement) or a catalytic angle (for ATP-hydrolysis measurement), the tweezers were turned on to stall the motor. The time required to travel from the pause angle to the stall angle was within 0.1 s. The image of rotary motion of the magnetic bead was recorded at 30 frames per second (FC300M, Takex) for the experiments shown in **Figures 2** and **3**, at 500 frames per second (HiD-Cam, Nac) for those in **Figure 4**, or at 1,000–3,000 frames per second (FASTCAM 1024PCI-SE, Photoron) for those in **Figure 4** and **Supplementary Figure 6**. Images were analyzed using custom-made software (Library).

Statistical analysis. We fitted the experimental results as shown in **Figures 2b** and **3a** using data analysis and graphing software (Origin 8.0, Originlab). The s.d. of parameter-value fitting are depicted as the error bars in **Figs. 2d–f** and **3b,c**. The s.d. of P_{ON} is given as $\sqrt{P_{ON}(100-P_{ON})/N}$, where N is the number of trials for each stall measurement.

Received 31 January 2011; accepted 1 September 2011; published online 20 November 2011

References

1. Frauenfelder, H., Sligar, S.G. & Wolynes, P.G. The energy landscapes and motions of proteins. *Science* **254**, 1598–1603 (1991).
2. Karplus, M. & Kuriyan, J. Molecular dynamics and protein function. *Proc. Natl. Acad. Sci. USA* **102**, 6679–6685 (2005).
3. Henzler-Wildman, K. & Kern, D. Dynamic personalities of proteins. *Nature* **450**, 964–972 (2007).
4. Bruice, T.C. & Benkovic, S.J. Chemical basis for enzyme catalysis. *Biochemistry* **39**, 6267–6274 (2000).
5. Koshland, D.E. Jr. Ray, W.J. Jr. & Erwin, M.J. Protein structure and enzyme action. *Fed. Proc.* **17**, 1145–1150 (1958).
6. Monod, J., Wyman, J. & Changeux, J.P. On the nature of allosteric transitions: a plausible model. *J. Mol. Biol.* **12**, 88–118 (1965).
7. Csermely, P., Palotai, R. & Nussinov, R. Induced fit, conformational selection and independent dynamic segments: an extended view of binding events. *Trends Biochem. Sci.* **35**, 539–546 (2010).

8. Boyer, P.D. The ATP synthase—a splendid molecular machine. *Annu. Rev. Biochem.* **66**, 717–749 (1997).
9. Cross, R.L. The rotary binding change mechanism of ATP synthases. *Biochim. Biophys. Acta* **1458**, 270–275 (2000).
10. Yoshida, M., Muneyuki, E. & Hisabori, T. ATP synthase—a marvellous rotary engine of the cell. *Nat. Rev. Mol. Cell Biol.* **2**, 669–677 (2001).
11. Senior, A.E., Nadanaciva, S. & Weber, J. The molecular mechanism of ATP synthesis by F_1F_o-ATP synthase. *Biochim. Biophys. Acta* **1553**, 188–211 (2002).
12. Noji, H., Yasuda, R., Yoshida, M. & Kinosita, K. Jr. Direct observation of the rotation of F_1-ATPase. *Nature* **386**, 299–302 (1997).
13. Abrahams, J.P., Leslie, A.G., Lutter, R. & Walker, J.E. Structure at 2.8-Å resolution of F_1-ATPase from bovine heart mitochondria. *Nature* **370**, 621–628 (1994).
14. Yasuda, R., Noji, H., Kinosita, K. Jr. & Yoshida, M. F_1-ATPase is a highly efficient molecular motor that rotates with discrete 120 degree steps. *Cell* **93**, 1117–1124 (1998).
15. Yasuda, R., Noji, H., Yoshida, M., Kinosita, K. Jr. & Itoh, H. Resolution of distinct rotational substeps by submillisecond kinetic analysis of F_1-ATPase. *Nature* **410**, 898–904 (2001).
16. Adachi, K. *et al.* Coupling of rotation and catalysis in F_1-ATPase revealed by single-molecule imaging and manipulation. *Cell* **130**, 309–321 (2007).
17. Shimabukuro, K. *et al.* Catalysis and rotation of F_1 motor: cleavage of ATP at the catalytic site occurs in 1 ms before 40 degree substep rotation. *Proc. Natl. Acad. Sci. USA* **100**, 14731–14736 (2003).
18. Watanabe, R., Iino, R. & Noji, H. Phosphate release in F_1-ATPase catalytic cycle follows ADP release. *Nat. Chem. Biol.* **6**, 814–820 (2010).
19. Itoh, H. *et al.* Mechanically driven ATP synthesis by F_1-ATPase. *Nature* **427**, 465–468 (2004).
20. Rondelez, Y. *et al.* Highly coupled ATP synthesis by F_1-ATPase single molecules. *Nature* **433**, 773–777 (2005).
21. Carter, N.J. & Cross, R.A. Mechanics of the kinesin step. *Nature* **435**, 308–312 (2005).
22. Gebhardt, J.C., Clemen, A.E., Jaud, J. & Rief, M. Myosin-V is a mechanical ratchet. *Proc. Natl. Acad. Sci. USA* **103**, 8680–8685 (2006).
23. Gennerich, A., Carter, A.P., Reck-Peterson, S.L. & Vale, R.D. Force-induced bidirectional stepping of cytoplasmic dynein. *Cell* **131**, 952–965 (2007).
24. Iko, Y., Tabata, K.V., Sakakihara, S., Nakashima, T. & Noji, H. Acceleration of the ATP-binding rate of F_1-ATPase by forcible forward rotation. *FEBS Lett.* **583**, 3187–3191 (2009).
25. Watanabe, R., Iino, R., Shimabukuro, K., Yoshida, M. & Noji, H. Temperature-sensitive reaction intermediate of F_1-ATPase. *EMBO Rep.* **9**, 84–90 (2008).
26. Spetzler, D. *et al.* Microsecond time scale rotation measurements of single F_1-ATPase molecules. *Biochemistry* **45**, 3117–3124 (2006).
27. Omote, H. *et al.* The γ-subunit rotation and torque generation in F_1-ATPase from wild-type or uncoupled mutant *Escherichia coli*. *Proc. Natl. Acad. Sci. USA* **96**, 7780–7784 (1999).
28. Hirono-Hara, Y., Ishizuka, K., Kinosita, K. Jr., Yoshida, M. & Noji, H. Activation of pausing F_1 motor by external force. *Proc. Natl. Acad. Sci. USA* **102**, 4288–4293 (2005).
29. Hirono-Hara, Y. *et al.* Pause and rotation of F_1-ATPase during catalysis. *Proc. Natl. Acad. Sci. USA* **98**, 13649–13654 (2001).
30. Sakaki, N. *et al.* One rotary mechanism for F_1-ATPase over ATP concentrations from millimolar down to nanomolar. *Biophys. J.* **88**, 2047–2056 (2005).
31. Noji, H. *et al.* Purine but not pyrimidine nucleotides support rotation of F_1-ATPase. *J. Biol. Chem.* **276**, 25480–25486 (2001).
32. Okuno, D., Iino, R. & Noji, H. Stiffness of γ subunit of F_1-ATPase. *Eur. Biophys. J.* **39**, 1589–1596 (2010).
33. Sielaff, H. *et al.* Domain compliance and elastic power transmission in rotary F_oF_1-ATPase. *Proc. Natl. Acad. Sci. USA* **105**, 17760–17765 (2008).
34. Uemura, S. & Ishiwata, S. Loading direction regulates the affinity of ADP for kinesin. *Nat. Struct. Biol.* **10**, 308–311 (2003).
35. Henzler-Wildman, K.A. *et al.* A hierarchy of timescales in protein dynamics is linked to enzyme catalysis. *Nature* **450**, 913–916 (2007).
36. Ikeguchi, M., Ueno, J., Sato, M. & Kidera, A. Protein structural change upon ligand binding: linear response theory. *Phys. Rev. Lett.* **94**, 078102 (2005).
37. Shimabukuro, K., Muneyuki, E. & Yoshida, M. An alternative reaction pathway of F_1-ATPase suggested by rotation without 80 degrees/40 degrees substeps of a sluggish mutant at low ATP. *Biophys. J.* **90**, 1028–1032 (2006).
38. von Ballmoos, C., Cook, G.M. & Dimroth, P. Unique rotary ATP synthase and its biological diversity. *Annu. Rev. Biophys.* **37**, 43–64 (2008).
39. Boyer, P.D., Cross, R.L. & Momsen, W. A new concept for energy coupling in oxidative phosphorylation based on a molecular explanation of the oxygen exchange reactions. *Proc. Natl. Acad. Sci. USA* **70**, 2837–2839 (1973).
40. Iino, R., Hasegawa, R., Tabata, K.V. & Noji, H. Mechanism of inhibition by C-terminal alpha-helices of the epsilon subunit of *Escherichia coli* F_oF_1-ATP synthase. *J. Biol. Chem.* **284**, 17457–17464 (2009).
41. Kinosita, K. Jr., Adachi, K. & Itoh, H. Rotation of F_1-ATPase: how an ATP-driven molecular machine may work. *Annu. Rev. Biophys. Biomol. Struct.* **33**, 245–268 (2004).
42. Nishizaka, T. *et al.* Chemomechanical coupling in F_1-ATPase revealed by simultaneous observation of nucleotide kinetics and rotation. *Nat. Struct. Mol. Biol.* **11**, 142–148 (2004).
43. Weber, J., Bowman, C. & Senior, A.E. Specific tryptophan substitution in catalytic sites of *Escherichia coli* F_1-ATPase allows differentiation between bound substrate ATP and product ADP in steady-state catalysis. *J. Biol. Chem.* **271**, 18711–18718 (1996).
44. Shimo-Kon, R. *et al.* Chemo-mechanical coupling in F_1-ATPase revealed by catalytic site occupancy during catalysis. *Biophys. J.* **98**, 1227–1236 (2010).
45. Senior, A.E. ATP synthase: motoring to the finish line. *Cell* **130**, 220–221 (2007).
46. Uchihashi, T., Iino, R., Ando, T. & Noji, H. High-speed atomic force microscopy reveals rotary catalysis of rotorless F_1-ATPase. *Science* **333**, 755–758 (2011).

Acknowledgments

We thank all members of the Noji laboratory. This work was partially supported by a Grant-in-Aid for Scientific Research (no. 18074005) to H.N. and by a Special Education and Research Expenses grant to H.N. from the Ministry of Education, Culture, Sports, Science and Technology, Japan.

Author contributions

R.W., D.O. and S.S. designed and performed experiments and analyzed data; K.S. gave technical support; R.I. and M.Y. gave technical support and conceptual advice; H.N. designed experiments, conceived the idea behind this paper and wrote this paper with R.W. and R.I.

Competing financial interests

The authors declare no competing financial interests.

Additional information

Supplementary information is available online at http://www.nature.com/naturechemicalbiology/. Reprints and permissions information is available online at http://www.nature.com/reprints/index.html. Correspondence and requests for materials should be addressed to H.N.